

Multi-objective Robust Planning for Self-sustained Highway Transportation Energy Systems Considering Spatial-temporal Distribution of Sources and Loads

Gen Zhao, Huaiyuan Zhang, Jianhua Wang, and Zhengyou He

Abstract—Constructing self-sustained highway transportation energy systems (HTESs) hinges on effective sustainable energy planning along highways. Addressing the complex spatial-temporal distribution characteristics of sources and loads presents a formidable challenge in accurately determining the siting and sizing of sustainable energy installations. In this study, we utilize a map rasterization approach and decentralized connection models for quantifying the spatial-temporal distribution characteristics of sources and loads. Leveraging these insights, the source-load-network cooperative operation models in uncertain scenarios, which seamlessly integrate highway and electricity networks, are built and embedded in the multi-objective robust planning model, enabling dynamic resource and demand management. The proposed planning model simultaneously optimizes the capacity, location, and connectivity of wind and photovoltaic power plants in HTES, while improving the robustness. Moreover, a multi-objective-oriented evaluation framework that adjusts the planning priorities based on three key dimensions – investment economy, self-sustained operation, and energy utilization efficiency – is formulated. The dynamic weight allocation mechanism enables tailored planning schemes that address diverse operational objectives effectively. Simulations of an actual HTES validate the effectiveness of the proposed planning model, demonstrating its capability to harmonize the inherent variabilities in the spatial-temporal distribution of sources and loads. The results highlight the significant variability in outcomes based on different objective orientations, underscoring the adaptability potential of the proposed planning model in designing futuristic HTES.

Index Terms—Highway transportation energy system, sustainable energy, robust planning, spatial-temporal distribution, siting and sizing, wind power plant, photovoltaic power plant.

I. INTRODUCTION

THE transportation sector consumes huge amounts of fossil energy and emits significant greenhouse gases, severely constraining the transition to energy cleanliness. According to data released by the International Energy Agency, the transportation industry consumes approximately 28% of the global energy and accounts for 23% of the global greenhouse gas emissions [1]. In the context of the Chinese “carbon peaking and carbon neutrality” targets [2], promoting the substitution of fossil energy and changing the pattern of energy consumption in the transportation sector are key solutions for meeting China’s commitment to carbon peaking and carbon neutrality. In addition, the planning outline of the national comprehensive and stereoscopic transportation network issued by the Chinese government states that it is necessary to promote the integrated development of transportation and energy networks [3]. In addition to these policies, the abundant clean energy along transportation routes provides favorable conditions for energy transition [4]. Consequently, the construction of a self-sustained clean energy supply framework adapted to transportation scenarios is a practical approach.

Among all transportation systems, the traditional highway transportation system is one of the most significant contributors to carbon emissions and requires an effective method to achieve energy cleanliness. With the increasing number of electric vehicles (EVs) and the vigorous development of sustainable energy technologies in recent years, most researchers have highlighted the rich resources along highways to construct self-sustained highway transportation energy systems (HTESs), thereby changing the way of energy supply on highways [4]. For instance, Bangladesh has begun to install bifacial photovoltaic (PV) power along highways [5]. In South Korea, numerous PV power systems have been installed on the roofs of on-street parking lots in rest areas and on slopes along highways [6]. China has built the world’s first PV highway on the Jinan South Ring Highway [7]. Although the above engineering projects indicate that there are numerous distributed sustainable energy resources along highways, the inherent source-load characteristics and diverse operational conditions in highway transportation sys-

Manuscript received: April 22, 2025; revised: June 19, 2025; accepted: August 25, 2025. Date of CrossCheck: August 25, 2025. Date of online publication: September 29, 2025.

This work was supported by the National Key R&D Program of China (No. 2022YFB2603100).

This article is distributed under the terms of the Creative Commons Attribution 4.0 International License (<http://creativecommons.org/licenses/by/4.0/>).

G. Zhao, H. Zhang (corresponding author), J. Wang, and Z. He are with the School of Electrical Engineering, Southwest Jiaotong University, Chengdu, China (e-mail: luckyz_888@163.com; zhang_huaiyuan@163.com; jhwang202302@163.com; hezy@swjtu.cn).

DOI: 10.35833/MPCE.2025.000257



tems present challenges for fully utilizing these resources. In addition, different planning schemes cause HTESs to exhibit distinct characteristics, which are reflected in various aspects such as energy capture, transmission, and consumption. Constructing a self-sustained HTES for different situations generally has different focuses on these aspects. Therefore, it is necessary to evaluate sustainable energy planning schemes from multiple perspectives, based on the relationship between energy supply and demand, from which the targeted planning schemes can be selected.

In recent years, with the large-scale development of EVs, researchers have begun to explore the use of clean energy on highways from the perspective of the planning and operation of charging stations. Reference [8] proposes a planning method for hybrid refueling stations that include PV and hydrogen allocation. This method is effective for meeting the demands of both EVs and fuel-driven vehicles. Reference [9] proposes a planning framework to realize the self-sustained operation of charging stations on highways, including the installation of PV panels and carbon capture and storage systems. In [10], a two-stage method is proposed for siting and sizing the standalone fully-renewable-powered charging stations on highways. Similarly, [11] realizes the site selection and capacity allocation of charging stations with integration of PV power and energy storage on highways. Reference [12] builds a hybrid energy management system containing PV power, wind power, and energy storage for highway chargers. However, the clean energy is only integrated into the charging stations to facilitate self-sustained operation at the station level in the above study. Studies on self-sustained solutions for the HTES are still scarce.

Although some researchers have conducted preliminary explorations into the construction of self-sustained HTES, some gaps still exist in current work. Instead of planning, most current studies have focused on the scheduling of self-sustained HTES. For instance, to enhance the operation of self-sustained HTES, the capability of mobile energy storage is applied to transfer energy in space and time in [13] and [14]. Reference [15] provides a self-sustained operation scheme for a highway rest-area energy system by integrating distributed PV power and energy storage. However, current studies on the planning of self-sustained HTES focus on local highway areas. Reference [16] proposes a configuration method for self-sustained microgrids for highway service areas. Reference [17] designs a wind-PV hybrid energy system based on the foldable umbrella mechanism, which can be installed in the medians of highways to simultaneously capture PV and wind energy. Reference [18] proposes a dynamic planning method for highway energy supply stations integrating charging and hydrogen refueling to cope with the growth in EV charging demand and the change in the proportion of hydrogen fuel cell vehicles. Reference [19] develops a zero-carbon energy system for highway service area by integrating renewable energy sources to replace grid electricity. These planning methods do not apply to the planning of the overall HTES. Specifically, for an overall HTES, the power load originates from multiple locations along highways, such as service areas, tunnels, route facilities, and toll stations.

Constructing a self-sustained HTES requires self-sustained schemes not only for local areas but also for the entire length of highways. Therefore, to realize the self-sustained operation of the overall HTES, the construction location, construction capacity, and connection nodes of sustainable energy power plants to electricity network are the key issues that need to be further investigated for sustainable energy planning. Therefore, it is necessary to study the sustainable energy planning schemes for an overall HTES, which are still lacking till now.

Several similar studies on the planning of sustainable energy resources in distribution networks provide references. For instance, the renewable energy capacity allocated to each node of a distribution network is optimized in [20] and [21]. Reference [22] proposes planning schemes for PV and wind power in distribution networks based on deep learning. Reference [23] builds a spatial-temporal carbon-response model to guide the planning of devices in distribution networks, thereby reducing carbon emissions. However, this model cannot be directly applied to HTES, as it fails to consider the effect of differences in the spatial-temporal distribution characteristics of sources and loads on planning schemes. Such an effect is significant for the overall HTES and cannot be ignored because of the long span of highway electricity networks. In addition, the aforementioned studies focus only on the economy of planning schemes. However, building a self-sustained HTES requires achieving the local use of clean energy, which requires evaluating planning schemes in terms of energy supply and energy consumption. In conclusion, to provide a rational planning scheme of sustainable energy for HTES, there is a need not only to further investigate the effect of source-load distribution characteristics along highways on planning schemes, but also to evaluate them from multiple perspectives.

Given the background and literature review presented above, this paper proposes a multi-objective robust planning model for HTES based on the spatial-temporal distribution of sources and loads. The key contributions of this study are summarized as follows.

- 1) The spatial-temporal distribution characteristics of the sources and loads are quantified using the map rasterization approach and decentralized connection model, respectively. Thus, the proposed planning model is effective in realizing the integrated optimization of the construction location, construction capacity, and connection nodes of sustainable energy power plants to electricity network.

- 2) The source-load-network cooperative operation models for HTES are developed. These sophisticated models incorporate the complex interactions between decentralized power generation within the electricity network and the distributed energy demands of the highway infrastructure, ensuring the optimal synergy between disparate elements of the energy ecosystem. By correlating these operation models in uncertain scenarios with the planning variables, we leverage the advantages of the two-stage robust optimization to enhance the robustness of the proposed planning model.

- 3) A multi-objective-oriented evaluation framework is proposed, which enhances the adaptability of the proposed plan-

ning model across three critical dimensions: investment economy, self-sustained operation, and energy utilization efficiency. By utilizing a dynamic weight allocation mechanism, this framework not only enables the proposed planning model to adapt to diverse operational requirements, but also provides bespoke planning schemes that are meticulously aligned with each strategic dimension. This nuanced evaluation framework is specifically designed to address the complexities and varied priorities of HTES, setting a new standard for multi-objective energy planning.

The remainder of this paper is organized as follows. Section II explains the problem description and motivation. Section III describes the multi-objective robust planning model for sustainable energy power plants. Section IV proposes the multi-objective-oriented evaluation framework. In Section V, a simulation is conducted on an actual HTES to verify the validity of the proposed planning model. Finally, Section VI

presents the conclusion.

II. PROBLEM DESCRIPTION AND MOTIVATION

The effective exploitation of sustainable energy resources along highways is key to achieving the self-sustained operation of HTES. However, the characteristics of long span and wide distribution cause the energy supply and demand in HTES to exhibit significant spatial-temporal distribution characteristics.

For example, Xixiang Highway is a pilot project in China for the integrated development of highways and energy [24]. As shown in Fig. 1, the abundance of wind and PV energy resources varies significantly at different locations along the highway, whereas major power consumers, including service areas, tunnels, route facilities, and toll stations, are distributed unevenly.

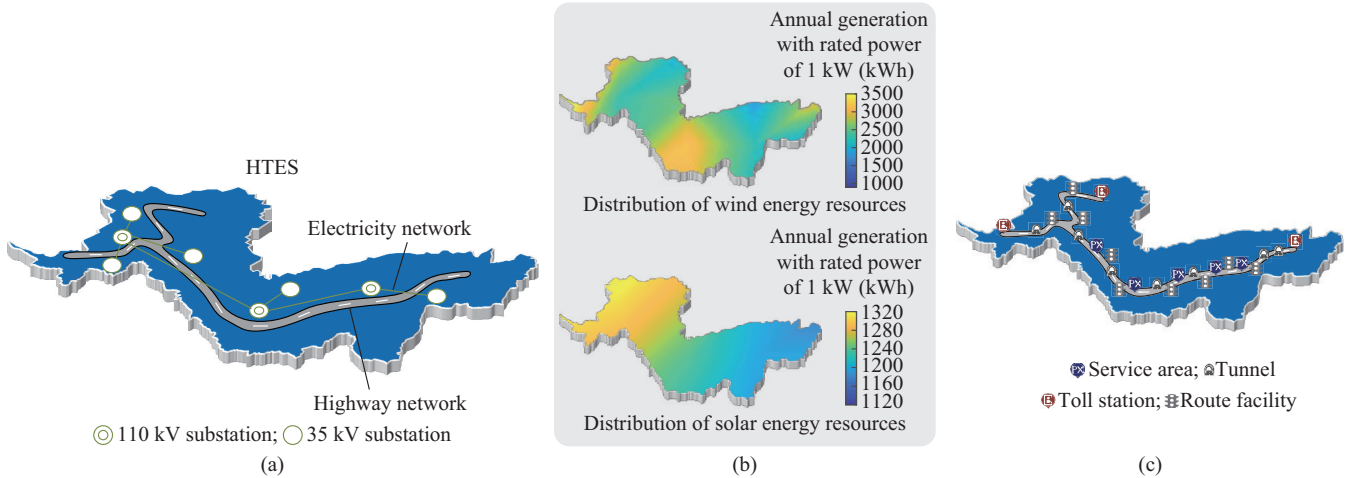


Fig. 1. Brief illustration of Xixiang Highway in China. (a) HTES structure. (b) Distribution of source. (c) Distribution of load.

In terms of highway loads, there are 136 km of tunnels, accounting for 58% of the total route length (233 km). Among them, there are eighteen extra-long tunnels (117 km), eight long tunnels (15 km), and seven short and medium tunnels (4 km). The highway includes five large service areas, three toll stations, and several facilities along its route. As the power grid around Xixiang Highway is weak with a low coverage level, it is difficult to supply adequate and reliable electricity for the large power demand of the entire highway. However, the abundance of sustainable energy in this area provides an effective solution. In addition, an independent electricity network including three 110 kV substations and five 35 kV substations has been constructed along the Xixiang Highway. By leveraging wind and PV energy to build power plants, this electricity network can serve as a channel for the integration, transmission, and consumption of sustainable energy [25].

III. MULTI-OBJECTIVE ROBUST PLANNING MODEL FOR SUSTAINABLE ENERGY POWER PLANTS

This section introduces a multi-objective robust planning model that ensures the strategic development of sustainable

energy within a self-sustained HTES. This model is intricately designed to harness the spatial-temporal distribution characteristics of sources and loads and is integrated seamlessly within the highway-electricity coupling network. By optimizing the installed capacity, construction location, and connection nodes of sustainable energy power plants to electricity network, this model realizes the comprehensive planning of energy infrastructure. Moreover, we develop multiple sophisticated objective functions that encapsulate investment economy, self-sustained operation, and energy utilization efficiency to guide the formulation of optimal energy planning schemes. The complex interplay of these objectives is meticulously orchestrated to produce tailored energy solutions that ensure the robustness and sustainability of system performance. The detailed architecture of the proposed planning model is presented in Supplementary Material A Fig. SA1, illustrating its integral role in shaping future HTES.

A. Source-load-network Cooperative Operation Models

A typical self-sustained HTES consists of sources, loads, and highway-electricity coupling networks. Specifically, the sustainable energy is used to enhance the self-sustained operation of HTES. The loads in the HTES are distributed along

the highway, mainly originating from service areas, tunnels, route facilities, and toll stations. In addition, the highway and electricity networks form a coupled relationship based on the spatial distribution of loads.

1) Source: Sustainable Energy Power Plants

Electricity in HTES is mainly provided by wind and PV power plants. Battery storage is used for power regulation.

1) Wind power plants

The wind speed measured at the ground monitoring station must be converted to the wind speed at the wind turbine rotor shaft, which is expressed as:

$$v_{i,s,t}^w = v_{i,s,t}^m (h_w/h_m)^a \quad (1)$$

where s is the index of scenario; t is the index of time; i is the index of power plant; $v_{i,s,t}^w$ is the wind speed at the wind turbine rotor hub; $v_{i,s,t}^m$ is the measured wind speed at the ground monitoring station; h_w is the height of wind turbine rotor hub; h_m is the height of ground monitoring station; and a is the surface roughness coefficient.

The output of wind power plants is expressed as [26]:

$$\tilde{P}_{i,s,t}^w = \begin{cases} 0 & v_{i,s,t}^w < v_{in}, v_{i,s,t}^w \geq v_{out} \\ \frac{v_{i,s,t}^w - v_{in}}{v_r - v_{in}} & v_{in} \leq v_{i,s,t}^w < v_r \\ 1 & v_r \leq v_{i,s,t}^w < v_{out} \end{cases} \quad (2)$$

$$(1 - \delta^w) \tilde{P}_{i,s,t}^w \leq P_{i,s,t}^w \leq (1 + \delta^w) \tilde{P}_{i,s,t}^w \quad (3)$$

$$0 \leq \Delta P_{i,s,t}^w \leq S_i^w P_{i,s,t}^w \quad (4)$$

$$0 \leq Q_{i,s,t}^w \leq \bar{Q}_{i,s,t}^w \quad (5)$$

where $P_{i,s,t}^w$ and $\tilde{P}_{i,s,t}^w$ are the maximum actual and predicted outputs of wind power per unit capacity, respectively; δ^w is the prediction error of wind power; $\Delta P_{i,s,t}^w$ is the wind power curtailment; S_i^w is the installed capacity of wind power plant; v_{in} , v_{out} , and v_r are the cut-in, cut-out, and rated wind speeds, respectively; and $Q_{i,s,t}^w$ and $\bar{Q}_{i,s,t}^w$ are the actual and maximum reactive power of wind power plant, respectively.

2) PV power plants

The output of PV power plants is expressed as [27]:

$$\tilde{P}_{i,s,t}^{pv} = I_{s,t} \phi [1 + \beta(T_{C,s,t} - T_{stc,s,t})] / I_{stc} \quad (6)$$

$$T_{C,s,t} = T_{temp,s,t} + (N_{oct} - 20) I_{s,t} / I_{stc} \quad (7)$$

$$(1 - \delta^{pv}) \tilde{P}_{i,s,t}^{pv} \leq P_{i,s,t}^{pv} \leq (1 + \delta^{pv}) \tilde{P}_{i,s,t}^{pv} \quad (8)$$

$$0 \leq \Delta P_{i,s,t}^{pv} \leq S_i^{pv} P_{i,s,t}^{pv} \quad (9)$$

$$0 \leq Q_{i,s,t}^{pv} \leq \bar{Q}_{i,s,t}^{pv} \quad (10)$$

where $P_{i,s,t}^{pv}$ and $\tilde{P}_{i,s,t}^{pv}$ are the maximum actual and predicted outputs of PV power per unit capacity, respectively; δ^{pv} is the prediction error of PV power; $\Delta P_{i,s,t}^{pv}$ is the PV power curtailment; $I_{s,t}$ is the radiation intensity; ϕ is the derating factor; S_i^{pv} is the installed capacity of PV power plant; β is the power-temperature coefficient; $T_{C,s,t}$ and $T_{stc,s,t}$ are the actual and standard operating temperatures, respectively; I_{stc} is the radiation intensity under standard test conditions; $T_{temp,s,t}$ is the environmental temperature; N_{oct} is the nominal temperature of PV cell; and $Q_{i,s,t}^{pv}$ and $\bar{Q}_{i,s,t}^{pv}$ are the actual and maximum reactive power of PV power plant, respectively.

3) Siting and sizing of sustainable energy power plants

Considering the spatial-temporal distribution characteristics of sustainable energy, a map rasterization approach is applied to determine the siting and sizing of wind and PV power plants [28]. This approach divides the planning area into N_{grid} rasters, as shown in Supplementary Material A Fig. SA2. Each raster is used as a candidate location for constructing sustainable energy power plants. Therefore, S_i^w and S_i^{pv} in each raster need to be optimized in the proposed planning model.

$$N_w = N_{pv} = N_{grid} \quad (11)$$

$$\begin{cases} 0 \leq S_i^w \leq \bar{S}_i^w \\ 0 \leq S_i^{pv} \leq \bar{S}_i^{pv} \end{cases} \quad (12)$$

where N_w and N_{pv} are the numbers of wind and PV power plants, respectively; and \bar{S}_i^w and \bar{S}_i^{pv} are the maximum capacities of wind and PV power plants in each raster, respectively.

Moreover, the battery storage is allocated to wind or PV power plants and it should satisfy the following constraints:

$$\bar{P}_i^{bs} = \eta S_i^{w/pv} \quad (13)$$

$$S_i^{bs} = \omega \bar{P}_i^{bs} \quad (14)$$

$$\begin{cases} soc_{i,s,t+1} = soc_{i,s,t} - P_{i,s,t}^{bs} \Delta t / S_i^{bs} & P_{i,s,t}^{bs} \leq 0 \\ soc_{i,s,t+1} = soc_{i,s,t} - P_{i,s,t}^{bs} \Delta t / (\eta_{dis} S_i^{bs}) & P_{i,s,t}^{bs} > 0 \end{cases} \quad (15)$$

$$-\bar{P}_i^{bs} \leq P_{i,s,t}^{bs} \leq \bar{P}_i^{bs} \quad (16)$$

$$-\bar{Q}_i^{bs} \leq Q_{i,s,t}^{bs} \leq \bar{Q}_i^{bs} \quad (17)$$

$$soc_{max}^{bs} \leq soc_{i,s,t}^{bs} \leq soc_{max}^{bs} \quad (18)$$

$$\sum_{t=1}^T P_{i,s,t}^{bs} \Delta t = 0 \quad (19)$$

$$bs \in \{w_bs, pv_bs\} \quad (20)$$

where the superscript bs = w_bs or pv_bs represents the battery storage allocated to wind or PV power plant, respectively; S_i^{bs} is the installed capacity of battery storage; η is the allocation rate; \bar{P}_i^{bs} and $P_{i,s,t}^{bs}$ are the maximum and actual charging/discharging power of battery storage, respectively; \bar{Q}_i^{bs} and $Q_{i,s,t}^{bs}$ are the maximum and actual reactive power of battery storage, respectively; ω is the charging time of battery storage; $soc_{i,s,t}$ is the state of charge of battery storage; η_c and η_{dis} are the charging and discharging efficiencies of battery storage, respectively; T is the total time; and Δt is the time interval.

When the location of a sustainable energy power plant is determined, the electricity network node nearest to the power plant is selected as the connection point.

$$L_i^{w/pv} = \min \{I_{i,n} | n = 1, 2, \dots, N_n\} \quad (21)$$

where $L_i^{w/pv}$ is the length of the grid-connected transmission lines for wind/PV power plant; $I_{i,n}$ is the distance between the wind/PV power plant and electricity network node n ; and N_n is the total number of electricity network nodes.

2) Load: Highway Transportation Load

In HTES, the load dynamics are uniquely characterized by their origins, i.e., service areas, tunnels, route facilities, and toll stations, which represent not only the core consumption

points in the system but also the complex interplay of energy demands across highway infrastructures. The distinct load distribution is pivotal because it shapes the strategic deployment of sustainable energy resources and informs the design of energy distribution models. Addressing the varied load characteristics is crucial for ensuring the efficiency and sustainability of HTES, making it a focal point in our system planning and optimization efforts.

1) Service area

The service area is an integrated energy system with multiple types of energy demands, including electricity, heat, cold, and gas loads [29], as shown in Supplementary Material A Fig. SA3. The conversion between different types of energy is achieved using electric boilers (EBs), electric cooling machines (ECMs), gas boilers (GBs), absorption refrigeration machines (ARMs), and power-to-gas (P2G). Different devices have different energy conversion efficiencies. Moreover, the energy storage such as electricity storage (ES) heat storage (HS), cold storage (CS), and gas storage (GS), is applied to enhance the energy balance. The balance between the supply and demand for multiple types of energy is expressed as:

$$A_g P_g + S_g = L_g \quad (22)$$

$$P_g = [P_{g,s,t}^{SA}, P_{g,s,t}^{EB}, P_{g,s,t}^{ECM}, P_{g,s,t}^{ARM}, P_{g,s,t}^{GB}, P_{g,s,t}^{P2G}, G_{g,s,t}]^T \quad (23)$$

$$S_g = [P_{g,s,t}^{ES}, P_{g,s,t}^{HS}, P_{g,s,t}^{CS}, P_{g,s,t}^{GS}]^T \quad (24)$$

$$L_g = [P_{g,s,t}^{eb} + P_{g,s,t}^{ev}, P_{g,s,t}^h, P_{g,s,t}^c, P_{g,s,t}^g]^T \quad (25)$$

$$A_g = \begin{bmatrix} 1 & -1 & -1 & 0 & 0 & -1 & 0 \\ 0 & \eta_{EB} & 0 & -1 & \eta_{GB} & 0 & 0 \\ 0 & 0 & \eta_{ECM} & \eta_{ARM} & 0 & 0 & 0 \\ 0 & 0 & 0 & 0 & -1 & \eta_{P2G} & \psi \end{bmatrix} \quad (26)$$

where g is the index of service area; A_g , P_g , S_g , and L_g are the matrices of energy conversion factors, output power, energy storage outputs, and energy loads, respectively; η_{EB} , η_{GB} , η_{ECM} , η_{ARM} , and η_{P2G} are the energy conversion efficiencies of EB, GB, ECM, ARM, and P2G, respectively; ψ is the calorific value of natural gas; $P_{g,s,t}^{SA}$ is the power supplied by an electricity network to a service area; $P_{g,s,t}^{EB}$, $P_{g,s,t}^{ECM}$, $P_{g,s,t}^{ARM}$, $P_{g,s,t}^{GB}$, and $P_{g,s,t}^{P2G}$ are the power consumed by EB, ECM, ARM, GB, and P2G, respectively; $G_{g,s,t}$ is the volume of the purchased natural gas; $P_{g,s,t}^{ES}$, $P_{g,s,t}^{HS}$, $P_{g,s,t}^{CS}$, and $P_{g,s,t}^{GS}$ are the output power of ES, HS, CS, and GS, respectively; $P_{g,s,t}^{eb}$ and $P_{g,s,t}^{ev}$ are the load power of building and charging power of EV, respectively; and $P_{g,s,t}^h$, $P_{g,s,t}^c$, and $P_{g,s,t}^g$ are the power of heat, cold, and gas loads, respectively.

These energy conversion devices and energy storage devices satisfy the following operational constraints.

$$0 \leq P_{g,s,t}^\theta \leq P_{g,s,t}^{\theta, \max} \quad \theta \in \{\text{EB, ECM, ARM, GB, P2G}\} \quad (27)$$

$$0 \leq |P_{g,s,t+1}^\theta - P_{g,s,t}^\theta| \leq \Delta P_{g,s,t}^{\theta, \max} \quad \theta \in \{\text{EB, ECM, ARM, GB}\} \quad (28)$$

$$-P_{g,s,t}^{\delta, \max} \leq P_{g,s,t}^\delta \leq P_{g,s,t}^{\delta, \max} \quad \delta \in \{\text{ES, HS, CS, GS}\} \quad (29)$$

$$E_{g,s,t+1}^\delta = \begin{cases} E_{g,s,t}^\delta - P_{g,s,t}^\delta \Delta t \eta_{ch}^\delta & P_{g,s,t}^\delta < 0, \delta \in \{\text{ES, HS, CS, GS}\} \\ E_{g,s,t}^\delta - P_{g,s,t}^\delta \Delta t / \eta_{dis}^\delta & P_{g,s,t}^\delta \geq 0, \delta \in \{\text{ES, HS, CS, GS}\} \end{cases} \quad (30)$$

$$E_{g,s,t}^{\delta, \min} \leq E_{g,s,t}^\delta \leq E_{g,s,t}^{\delta, \max} \quad (31)$$

$$E_{g,s,T}^\delta = E_{g,0}^\delta \quad (32)$$

where θ is the index of energy conversion device; δ is the index of energy storage device; $P_{g,s,t}^\theta$ and $P_{g,s,t}^{\delta, \max}$ are the maximum output power of energy conversion device and energy storage device, respectively; $\Delta P_{g,s,t}^{\theta, \max}$ is the maximum climbing power of energy storage device; $E_{g,s,t}^\delta$ is the storage amount of energy storage device; η_{dis}^δ and η_{ch}^δ are the energy release and energy storage coefficients of energy storage device, respectively; $E_{g,s,t}^{\delta, \max}$ and $E_{g,s,t}^{\delta, \min}$ are the maximum and minimum storage amounts of energy storage device, respectively; and $E_{g,0}^\delta$ is the initial storage amount of energy storage device.

With the increasing number of EVs, its charging power $P_{g,s,t}^{ev}$ in service areas has become an important component. However, the charging load exhibits disorderliness and uncertainties owing to numerous combinations of multiple factors such as arrival time, charging duration, driving distance, and energy consumption per kilometer. Moreover, a limited number of charging piles may cause queuing problems. Therefore, to address these problems, we formulate a charging load simulation process that integrates the uncertainty and queuing problems, as presented in Supplementary Material B. By leveraging the Monte Carlo algorithm, this process effectively characterizes the stochastic charging behaviors of EVs, whereas the queuing models are embedded in this process depending on the number of charging piles.

The highway and electricity networks are coupled to each other. Electricity generated by sustainable energy power plants flows to the load side through the electricity network transmission. To effectively select the connection nodes of sustainable energy power plants, it is necessary to determine the power that the electricity network needs to supply to the service areas, i.e., $P_{g,s,t}^{SA}$. However, as discussed above, the total electricity demand of service area cannot be directly obtained because of the conversion between different types of energy in the service area. Therefore, an operation model that optimizes the power allocation of multiple types of energy is constructed to obtain the optimal value of $P_{g,s,t}^{SA}$.

$$\begin{cases} \min C_g = \sum_{s=1}^{N_s} \sum_{t=1}^T \sum_{\theta} c_\theta P_{g,s,t}^\theta + \sum_{s=1}^{N_s} \sum_{t=1}^T \sum_{\delta} c_\delta |P_{g,s,t}^\delta| + \sum_{s=1}^{N_s} \sum_{t=1}^T c_G G_{g,s,t} \\ \text{s.t. } \theta = \{\text{EB, ECM, ARM, GB, P2G}\} \\ \delta = \{\text{ES, HS, CS, GS}\} \end{cases} \quad (22)-(32) \quad (33)$$

where C_g is the total operation cost of service area; c_θ and c_δ are the unit operation costs of energy conversion device and energy storage device, respectively; c_G is the unit purchase cost of natural gas; and N_s is the number of scenarios.

2) Tunnel

The electrical equipment in tunnels includes ventilation, lighting, and monitoring systems. A typical intraday load curve of tunnels is shown in Supplementary Material A Fig. SA4. The power demand of tunnels can be expressed as:

$$P_{k,s,t}^T = L_k^T p_{T,t}^{T, \text{typical}} \quad (34)$$

where $P_{k,s,t}^T$ is the power demand of the k^{th} tunnel; L_k^T is the length of the k^{th} tunnel; p_T is the power demand per kilometer of tunnel; and P_T^{typical} is a typical power demand of tunnels.

3) Route facility

The core of HTES design lies in the route facilities that include an array of essential monitors and signals strategically distributed along the highway. These facilities are not merely functional components. They represent critical nodes of continuous energy demand to ensure the safety and efficiency of highway management. Therefore, the power demand of route facilities is shown as:

$$P_{k,s,t}^{\text{RF}} = p_{\text{RF}} L_k \quad (35)$$

where $P_{k,s,t}^{\text{RF}}$ is the power demand of the k^{th} section of highway; p_{RF} is the power demand per kilometer of highway; and L_k is the length of the k^{th} section of highway.

The focus on route facilities underscores their pivotal role in maintaining the operational integrity and sustainability of HTES, marking a significant advancement in the domain of highway energy management.

4) Toll station

Toll stations generally require 24-hour uninterrupted power supply with little or no fluctuation. The power demand of the m^{th} toll station can be expressed as a constant value P_m^{TS} .

3) Network: Highway-electricity Coupling Networks

In HTES, the sustainable energy power plants are connected to electricity network nodes to feed power, whereas loads at different locations in the highway network are connected to different nodes to obtain power from the electricity network. In this context, the power is allocated among multiple lines to satisfy the power demands of each node. Therefore, to characterize the coupling of the electricity and highway networks in HTES, the following models are constructed based on LinDistFlow models [30].

$$P_{n,s,t}^{\text{source}} = \sum_{l \in \Omega_n} P_{l,s,t} + P_{n,s,t}^{\text{load}} \quad (36)$$

$$Q_{n,s,t}^{\text{source}} = \sum_{l \in \Omega_n} Q_{l,s,t} + Q_{n,s,t}^{\text{load}} \quad (37)$$

$$-\bar{P}_l \leq P_{l,s,t} \leq \bar{P}_l \quad (38)$$

$$-\bar{Q}_l \leq Q_{l,s,t} \leq \bar{Q}_l \quad (39)$$

$$0 \leq P_{n,s,t}^{\text{g}} \leq u_n^{\text{g}} \bar{P}^{\text{g}} \quad u_n^{\text{g}} \in \{0, 1\} \quad (40)$$

$$0 \leq Q_{n,s,t}^{\text{g}} \leq u_n^{\text{g}} \bar{Q}^{\text{g}} \quad u_n^{\text{g}} \in \{0, 1\} \quad (41)$$

$$U_{n,s,t} = k_{nn'}^2 U_{n',s,t} - 2(R_{nn'} P_{n',s,t} + X_{nn'} Q_{n',s,t}) \quad (42)$$

$$U_{n,\min}^2 \leq U_{n,s,t} \leq U_{n,\max}^2 \quad (43)$$

$$P_{n,s,t}^{\text{source}} = \sum_{i=1}^{N_n^{\text{w}}} (S_i^{\text{w}} P_{i,s,t}^{\text{w}} - \Delta P_{i,s,t}^{\text{w}} + P_{i,s,t}^{\text{w,es}}) + \sum_{i=1}^{N_n^{\text{pv}}} (S_i^{\text{pv}} P_{i,s,t}^{\text{pv}} - \Delta P_{i,s,t}^{\text{pv}} + P_{i,s,t}^{\text{pv,es}}) + P_{n,s,t}^{\text{g}} \quad (44)$$

$$Q_{n,s,t}^{\text{source}} = \sum_{i=1}^{N_n^{\text{w}}} (Q_{i,s,t}^{\text{w}} + Q_{i,s,t}^{\text{w,es}}) + \sum_{i=1}^{N_n^{\text{pv}}} (Q_{i,s,t}^{\text{pv}} + Q_{i,s,t}^{\text{pv,es}}) + Q_{n,s,t}^{\text{g}} \quad (45)$$

$$\tilde{P}_{n,s,t}^{\text{load}} = P_{n,s,t}^{\text{SA}} + P_{n,s,t}^{\text{T}} + P_{n,s,t}^{\text{RF}} + P_{n,s,t}^{\text{TS}} + P_{n,s,t}^{\text{RL}} \quad (46)$$

$$(1 - \delta^{\text{load}}) \tilde{P}_{n,s,t}^{\text{load}} \leq P_{n,s,t}^{\text{load}} \leq (1 + \delta^{\text{load}}) \tilde{P}_{n,s,t}^{\text{load}} \quad (47)$$

where Ω_n is the set of lines connected with node n ; $P_{l,s,t}$ and $Q_{l,s,t}$ are the active and reactive power of line l , respectively; \bar{P}_l and \bar{Q}_l are the maximum active and reactive power of line l , respectively; $P_{n,s,t}^{\text{source}}$ and $P_{n,s,t}^{\text{load}}$ are the active power of source and load at node n , respectively; $Q_{n,s,t}^{\text{source}}$ and $Q_{n,s,t}^{\text{load}}$ are the reactive power of source and load at node n , respectively; $U_{n,s,t}$ ($U_{n',s,t}$) is the square of voltage at node n (n'); $R_{nn'}$ and $X_{nn'}$ are the resistance and reactance of line nn' , respectively; U_n^{max} and U_n^{min} are the maximum and minimum voltages at node n , respectively; $k_{nn'}$ is the voltage ratio between node n and node n' ; N_n^{w} and N_n^{pv} are the numbers of wind and PV power plants connected to node n , respectively; $P_{n,s,t}^{\text{g}}$ and $Q_{n,s,t}^{\text{g}}$ are the active and reactive power flowing into node n from the upper power grid, respectively; u_n^{g} denotes whether the node n is connected to the upper power grid; \bar{P}^{g} and \bar{Q}^{g} are the maximum active and reactive power from the upper power grid, respectively; $P_{n,s,t}^{\text{SA}}$, $P_{n,s,t}^{\text{T}}$, $P_{n,s,t}^{\text{RF}}$, $P_{n,s,t}^{\text{TS}}$ and $P_{n,s,t}^{\text{RL}}$ are the loads of service area, tunnel, route facility, toll station, and residential area at node n , respectively; $\tilde{P}_{n,s,t}^{\text{load}}$ is the predicted load power; and δ^{load} is the predicted load error.

B. Objective Functions from Multiple Perspectives

In this paper, we develop multiple objective functions that are core to the HTES planning model. These functions are tailored from three strategic perspectives: investment economy, self-sustained operation, and energy utilization efficiency.

1) Minimizing Investment Cost

To optimize the investment economy, the objective function f_1 aims to minimize the total investment cost C_{inv} :

$$\min f_1 = C_{\text{inv}} \quad (48)$$

$$C_{\text{inv}} = (\alpha c_w + e_w) \sum_{i=1}^{N_w} S_i^{\text{w}} + (\alpha c_{\text{pv}} + e_{\text{pv}}) \sum_{i=1}^{N_{\text{pv}}} S_i^{\text{pv}} + \sum_{i=1}^{N_w + N_{\text{pv}}} (c_s S_i^{\text{es}} + c_p \bar{P}_i^{\text{es}}) \quad (49)$$

$$\alpha = \frac{\vartheta(1 + \vartheta)^y}{(1 + \vartheta)^y - 1} y \quad (50)$$

where c_w and c_{pv} are the construction costs of wind and PV power plants, respectively; e_w and e_{pv} are the operation costs of wind and PV power plants, respectively; c_s and c_p are the investment costs for capacity and power of energy storage, respectively; ϑ is the depreciation rate; and y is the project year.

2) Maximizing Self-sustained Rate

To optimize the self-sustained operation, the objective function f_2 aims to maximize the self-sustained rate.

$$\max f_2 = \frac{1}{N_s} \sum_{s=1}^{N_s} \frac{\sum_{i=1}^{N_{\text{pv}}} \sum_{t=1}^T (S_i^{\text{pv}} P_{i,s,t}^{\text{pv}} - \Delta P_{i,s,t}^{\text{pv}}) + \sum_{i=1}^{N_w} \sum_{t=1}^T (S_i^{\text{w}} P_{i,s,t}^{\text{w}} - \Delta P_{i,s,t}^{\text{w}})}{\sum_{n=1}^{N_n} \sum_{t=1}^T P_{n,s,t}^{\text{load}}} \quad (51)$$

Electricity sources in HTES can be divided into sustainable energy power plants and an upper power grid. Maximizing the self-sustained rate of HTES means maximizing the

share of sustainable energy generation for loads and minimizing the amount of electricity supplied from the upper power grid. Therefore, (51) can be converted into:

$$\min C_g = c_{\text{buy}} \sum_{s=1}^{N_s} \sum_{t=1}^T \sum_{n=1}^{N_n} P_{n,s,t}^g \quad (52)$$

where C_g is the cost of electricity purchased from the upper power grid; and c_{buy} is the unit cost of electricity.

3) Maximizing Energy Utilization Rate

To optimize the energy utilization, the objective function f_3 aims to maximize the energy utilization rate.

$$\max f_3 = \frac{1}{N_s} \sum_{s=1}^{N_s} \left(1 - \frac{\sum_{i=1}^{N_{pv}} \sum_{t=1}^T \Delta P_{i,s,t}^{pv} + \sum_{i=1}^{N_n} \sum_{t=1}^T \Delta P_{i,s,t}^w}{\sum_{i=1}^{N_{pv}} \sum_{t=1}^T S_i^{pv} P_{i,s,t}^{pv} + \sum_{i=1}^{N_n} \sum_{t=1}^T S_i^w P_{i,s,t}^w} \right) \quad (53)$$

Maximizing the energy utilization rate of HTES means maximizing the share of actual sustainable energy generation and minimizing the amount of sustainable energy curtailment. Therefore, (53) can be converted into:

$$\min C_c = c_{\text{cur}} \sum_{s=1}^{N_s} \left(\sum_{i=1}^{N_n} \sum_{t=1}^T \Delta P_{i,s,t}^w + \sum_{i=1}^{N_{pv}} \sum_{t=1}^T \Delta P_{i,s,t}^{pv} \right) \quad (54)$$

where C_c and c_{cur} are the total and unit costs of the sustainable energy curtailment, respectively.

The tripartite method reflects a substantial analytical and computational endeavor, underscoring the innovation inherent in the proposed planning model and representing a significant advancement. Through this method, we enable planners and stakeholders to dynamically adjust the planning parameters to meet specific operational targets, showcasing the adaptability and forward-thinking design of the proposed planning model.

C. Two-stage Robust Optimization

Considering the uncertainties of wind, PV, and load power, the box uncertainty set can be established as:

$$\begin{aligned} \Phi: &= \{U_{i,s,t}^w \in [(1-\delta^w)\tilde{P}_{i,s,t}^w, (1+\delta^w)\tilde{P}_{i,s,t}^w], \\ &P_{i,s,t}^{pv} \in [(1-\delta^{pv})\tilde{P}_{i,s,t}^{pv}, (1+\delta^{pv})\tilde{P}_{i,s,t}^{pv}], \\ &P_{n,s,t}^{\text{load}} \in [(1-\delta^{\text{load}})\tilde{P}_{n,s,t}^{\text{load}}, (1+\delta^{\text{load}})\tilde{P}_{n,s,t}^{\text{load}}]\} \end{aligned} \quad (55)$$

$$U = [P_{i,s,t}^w, P_{i,s,t}^{pv}, P_{n,s,t}^{\text{load}}]^T \quad (56)$$

Equations (55) and (56) indicate that the actual value is equal to the predicted value plus the uncertain prediction error. Accordingly, a two-stage robust optimization is proposed to ensure that the uncertain scenarios are adopted. In the first stage, the installed capacities of wind and PV power plants are optimized to minimize the total investment cost. Based on the results in the first stage, the second stage aims to minimize the operation cost in the worst-case scenario with uncertainties. The complete planning model with the objective function f is expressed as:

$$\begin{cases} \min f = \omega_1 C_{\text{inv}} + \max \min (\omega_2 C_g + \omega_3 C_c) \\ \text{s.t. (1)-(21), (34)-(47)} \end{cases} \quad (57)$$

where ω_1 , ω_2 , and ω_3 are the weights of the investment economy, self-sustained rate, and utilization rate, respectively.

The model in (57) is expressed in compact form as:

$$\begin{cases} \min_X \{C^T X + \max_{U \in \Phi} \min_Y B^T Y\} \\ X = [S_i^w, S_i^{pv}, P_{i,s,t}^{w,es}, P_{i,s,t}^{pv,es}, Q_{i,s,t}^{pv,es}, Q_{i,s,t}^{w,es}]^T \\ Y = [\Delta P_{i,s,t}^w, \Delta P_{i,s,t}^{pv}, Q_{i,s,t}^w, Q_{i,s,t}^{pv}, P_{n,s,t}^g, Q_{n,s,t}^g, P_{nn',s,t}, Q_{nn',s,t}, U_{i,s,t}]^T \\ \text{s.t. } DX \geq d \\ EX = 0 \\ FY \geq GU + e \\ HY + (J + KX)U + IX = 0 \end{cases} \quad (58)$$

where X is the variable vector in the first stage; Y is the variable vector in the second stage; C and B are the column vectors of the coefficients that correspond to the objective function in (57); D , E , F , G , H , J , K , and I are the coefficient matrices of variables under the corresponding constraints; and d and e are the constant vectors. The first constraint in (58) corresponds to (12) and (16)-(18). The second constraint in (58) corresponds to (19). The third constraint in (58) corresponds to (4), (5), (9), (10), (38)-(41), and (43). The fourth constraint in (58) corresponds to (36), (37), and (42).

By leveraging the column-and-constraint generation (C&CG) algorithm [31], (58) can be decomposed into a master problem and subproblem for an effective solution.

The master problem is formulated as:

$$\begin{cases} \min_X \{C^T X + \phi\} \\ \text{s.t. } \phi \geq B^T Y_r \\ DX \geq d \\ EX = 0 \\ FY_r \geq GU_r^* + e \\ HY_r + (J + KX)U_r^* + IX = 0 \end{cases} \quad (59)$$

where ϕ is the intermediate variable; r is the index of iterations; and U_r^* is the value of U in the worst-case scenario after the r^{th} iteration.

The subproblem is formulated as (60). It is a two-layer model that can be converted into a single-layer model for an effective solution using the Karush-Kuhn-Tucker condition [32].

$$\begin{cases} \max_{U \in \Phi} \min_Y B^T Y \\ \text{s.t. } FY \geq GU + e \\ HY + (J + KX^*)U + IX^* = 0 \end{cases} \quad (60)$$

where X^* is the value of X solved by (59).

The specific solution process of C&CG algorithm is given as follows.

Step 1: initialize the uncertainty parameters in the worst-case scenario as U_0 . The upper boundary $UB = +\infty$ and the lower boundary $LB = -\infty$ are set. Set $r = 0$.

Step 2: solve the master problem (59) based on U_0 to derive the optimal solution $(X_{r+1}^*, \phi_{r+1}^*, Y_1^*, Y_2^*, \dots, Y_r^*)$. Update $LB = \max\{LB, \phi_{r+1}^*\}$.

Step 3: insert X_{k+1}^* into (60) to solve the subproblem. Derive the optimal value $B^T Y_{r+1}^*$ and uncertainty parameters in the worst-scenario U_{r+1} . Update $UB = \min\{UB, B^T Y_{r+1}^*\}$.

Step 4: if $UB-LB \leq \varepsilon$ exists, return X_{r+1}^* and Y_{r+1}^* ; otherwise, the variable Y_{r+1} is created and the following constraints are added to the master problem (59). Update $r=r+1$ and go to *Step 2*.

$$\begin{cases} \phi \geq \mathbf{B}^T \mathbf{Y}_{r+1} \\ \mathbf{F} \mathbf{Y}_{r+1} \geq \mathbf{G} \mathbf{U}_{r+1}^* + \mathbf{e} \\ \mathbf{H} \mathbf{Y}_{r+1} + (\mathbf{J} + \mathbf{K} \mathbf{X}) \mathbf{U}_{r+1}^* + \mathbf{I} \mathbf{X} = 0 \end{cases} \quad (61)$$

IV. MULTI-OBJECTIVE-ORIENTED EVALUATION FRAMEWORK

In this section, a multi-objective-oriented evaluation framework is proposed based on the analytical hierarchy process (AHP) [33], to determine the weights of the three objectives according to different planning requirements.

A. Structure of Multi-objective-oriented Evaluation Framework

Based on the analytical concept of decomposition followed by integration, the multi-objective-oriented evaluation framework is decomposed into three layers, as shown in Fig. 2. The optimal objective function f in (57) is the problem to be solved and is chosen as the target layer. From (48)-(54), the factors affecting the target layer can be summarized as installed capacity A_1 , electricity from the upper power grid A_2 , load demand A_3 , sustainable energy generation A_4 , and resource endowment A_5 . These factors constitute the criterion layer of this evaluation framework. The scheme layer includes three planning objectives: investment economy B_1 , self-sustained rate B_2 , and energy utilization rate B_3 . Finally, the weights of the three planning objectives in the objective function f are determined based on the influence relationships among the three layers.

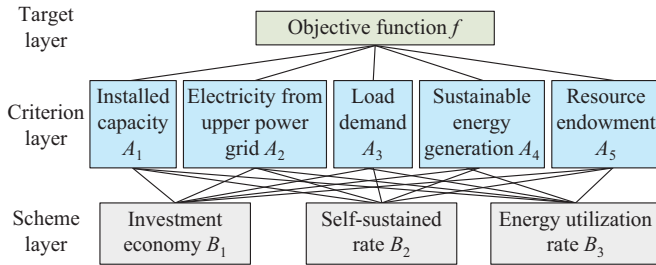


Fig. 2. Structure of multi-objective-oriented evaluation framework.

B. Weight Allocation Mechanism

By analyzing the interrelationships between neighboring layers, the final weights indicating the importance of different objectives in the scheme layer relative to the target layer could be determined.

1) Construction of Judgment Matrices

In this part, two judgment matrices are created. The first judgment matrix indicates the importance of factors in the criterion layer relative to the target layer, and the importance levels are different when oriented toward different planning objectives:

$$X_{\delta} = [a_{x,y}]_{N_A \times N_A} \quad (62)$$

where X_{δ} is the judgment matrix of criterion layer relative to target layer oriented toward the planning objective δ ; $a_{x,y}$ is the importance level of A_x compared with A_y relative to the target layer, and its value is given in Supplementary Material A Table SAI; and N_A is the number of factors in the criterion layer.

The second judgment matrix Y_{A_j} represents the importance of elements in the scheme layer relative to A_j in the criterion layer, which is relatively objective and generally does not change when the subjectively oriented objective changes.

$$Y_{A_j} = [b_{x,y}]_{N_B \times N_B} \quad (63)$$

where $b_{x,y}$ is the importance level of B_x compared with B_y relative to A_j in the criterion layer, and its value is given in Supplementary Material A Table SAI; and N_B is the number of factors in the scheme layer.

2) Consistency Test of Judgment Matrices

A consistency test is necessary to check whether the construction of the judgment matrices X_{δ} and Y_{A_j} is effective, which is expressed in Supplementary Material C.

3) Weight Determination

The maximum characteristic roots λ_{\max}^X and λ_{\max}^Y of X_{δ} and Y_{A_j} are used to calculate their eigenvectors, respectively, which are normalized to the weight vector of the criterion layer relative to target layer $\mathbf{W}_{\delta}^{C-T} = [\omega_{A_1}^{C-T}]^T$ and the weight vector of scheme layer relative to the criterion layer $\mathbf{W}^{S-A_j} = [\omega_{B_x}^{S-A_j}]$.

$$\begin{cases} X_{\delta} \mathbf{W}_{\delta}^{C-T} = \lambda_{\max}^X \mathbf{W}_{\delta}^{C-T} \\ Y_{A_j} \mathbf{W}^{S-A_j} = \lambda_{\max}^Y \mathbf{W}^{S-A_j} \end{cases} \quad (64)$$

$$\mathbf{W}_{\delta}^{C-T} = [\omega_{A_1}^{C-T}, \omega_{A_2}^{C-T}, \omega_{A_3}^{C-T}, \omega_{A_4}^{C-T}, \omega_{A_5}^{C-T}]^T \quad (65)$$

$$\mathbf{W}^{S-A_j} = [\omega_{B_1}^{S-A_j}, \omega_{B_2}^{S-A_j}, \omega_{B_3}^{S-A_j}]^T \quad (66)$$

Finally, the vector $\mathbf{W}_{\delta}^{S-T}$ including the weights of three planning objectives ω_1 - ω_3 in the objective function is determined as:

$$\mathbf{W}_{\delta}^{S-T} = [\omega_1, \omega_2, \omega_3] = (\mathbf{W}_{\delta}^{C-T})^T (\mathbf{W}^{S-C})^T \quad (67)$$

$$\mathbf{W}^{S-C} = [\mathbf{W}^{S-A_1}, \mathbf{W}^{S-A_2}, \mathbf{W}^{S-A_3}, \mathbf{W}^{S-A_4}, \mathbf{W}^{S-A_5}] \quad (68)$$

V. SIMULATION RESULTS AND DISCUSSION

The proposed planning model is applied to the Xixiang Highway in China, as shown in Fig. 3. To support the simulation, the real-world meteorological data on the wind speed, solar radiation, and temperature are obtained from the NASA meteorological database MERRA-2 [34]. Based on these data, the map rasterization approach processes the studied area into 25 rasters with a precision of $0.25^{\circ} \times 0.25^{\circ}$. To characterize the source-load fluctuation, the typical intraday outputs of wind and PV power as well as the typical intraday demand of loads on weekdays and holidays in spring, summer, autumn, and winter, are obtained using the K -means clustering algorithm, as shown in Supplementary Material A Fig. SA5. Table I lists the parameter settings. The charging power curves of five service areas in different scenarios are shown in Supplementary Material B Fig. SB2.

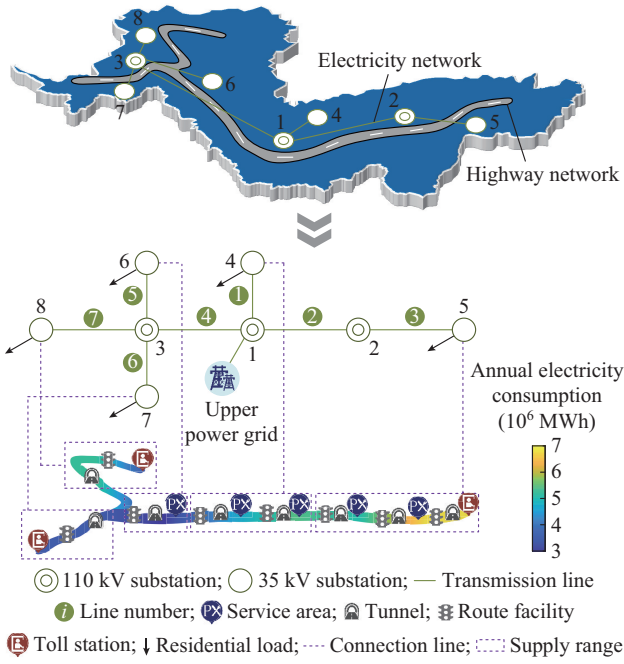


Fig. 3. Schematic diagram of coupling between highway network and electricity network.

TABLE I
PARAMETER SETTINGS

Category	Symbol	Value
Wind power plant	v_{in}	3 m/s
	v_{out}	25 m/s
	v_r	11 m/s
	h_w	70 m
	c_w	1209 \$/kW
	e_w	50 \$/kW
PV power plant	ϕ	0.7
	β	-0.0045%/°C
	$T_{stc,s,t}$	25 °C
	N_{oct}	46.5 °C
	c_{pv}	675 \$/kW
Highway	e_{pv}	10 \$/kW
	p_T	20 kW/km
	p_{RF}	1 kW/km
Other	p_m^{TS}	15 kW
	c_{buy}	0.069 \$/kWh
	c_{cur}	0.138 \$/kWh
	c_s	138 \$/kW
	c_p	413 \$/kWh
	r	0.05
	y	20 years

The optimization model is implemented on a laptop computer with an Intel Core i9-12900K CPU (3.20 GHz) and solved using the MIP solver CPLEX via MATLAB 2022a with the YALMIP toolbox.

A. Multi-objective-oriented Weight Allocation

To analyze the differences of the proposed planning model

oriented toward different objectives, the following four planning schemes are set. ① Scheme 0 (S0): with no sustainable energy; ② Scheme 1 (S1): oriented toward investment economy; ③ Scheme 2 (S2): oriented toward self-sustained rate; and ④ Scheme 3 (S3): oriented toward energy utilization rate.

Based on the multi-objective-oriented evaluation framework, the judgment matrices are constructed for S1, S2, and S3. For S1, the installed capacity is more important in the objective function. For S2, the electricity from the upper power grid and the load demand are more important in the objective function. For S3, the sustainable energy generation and resource endowment are more important in the objective function. Therefore, based on the importance of each element when oriented toward different objectives as described above, the judgment matrices X_δ oriented toward different objectives are constructed in Supplementary Material C. Besides, the values of matrices Y_{A_i} are almost constant for different goal orientations, as shown in Supplementary Material C. Then, the solutions of final weights can be derived, as listed in Table II. The results indicate that, when oriented toward a certain goal, the corresponding weight is greater.

TABLE II
SOLUTIONS OF FINAL WEIGHTS

Scheme	ω_1	ω_2	ω_3
S1	0.4017	0.3655	0.2328
S2	0.1489	0.5064	0.3447
S3	0.1451	0.3412	0.5137

B. Robustness Analysis

The proposed planning model is solved under S1-S3, with a favorable convergence performance, as shown in Fig. 4. Specifically, the upper and lower boundaries converge after approximately 15 iterations, confirming the computational validity of the proposed planning model. To further examine the robustness, the wind and PV power plants planned in the 18th grid under S2 as well as the load at node 4 are analyzed. As shown in Fig. 5, the actual values lie near the boundaries of the uncertainty interval. This is because the model in (58) aims to determine the optimal solution in the worst-case scenario with multiple uncertainties, which corresponds to the maximum objective of the second stage in (58). During hours 1-11 and 20-24, the actual values of wind and PV power lie on the lower boundary of the uncertainty interval, whereas the actual value of load power lies on the upper boundary of the uncertainty interval, which leads to a higher electricity purchase cost in the second stage. This reflects the worst-case scenario. During hours 12-19, the actual values of wind and PV power lie on the upper boundary of the uncertainty interval, whereas the actual value of load power lies on the lower boundary of the uncertainty interval, which leads to a higher power curtailment cost in the second stage. This also reflects the worst-case scenario. The above results indicate that the proposed planning model can design planning schemes that consider the worst-case scenario with multiple uncertainties, thereby enhancing the robustness.

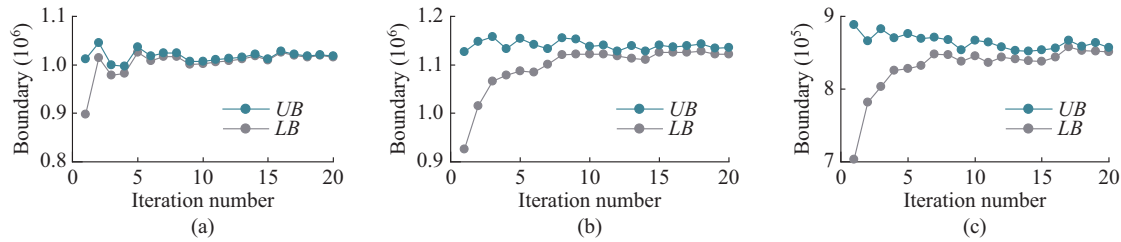


Fig. 4. Convergence performance of proposed planning model. (a) S1. (b) S2. (c) S3.

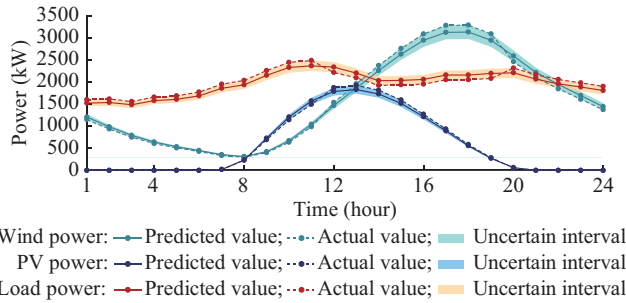


Fig. 5. Predicted and actual values of wind, PV, and load power.

C. Analysis of Planning Schemes

The installed capacity of wind and PV power plants constructed in each raster under S1-S3 is listed in Table III. Table IV lists the values of multiple objectives under S0-S3. First, the total costs under S1-S3 are all lower than that under S0, which indicates that constructing sustainable energy power plants for HTES not only promotes energy cleanliness but also improves the economy. In particular, S1 provides the smallest installed capacity of sustainable energy power plants. Consequently, the investment cost under S1 ($\$1.25 \times 10^6$) is the lowest compared with that under S2 ($\$2.04 \times 10^6$) and S3 ($\1.62×10^6). Besides, the sustainable energy power plants are almost running at the maximum power output to meet the large power demand, which makes S1 maintain the highest energy utilization rate (99.68%). However, the smallest installed capacity results in the lowest sustainable energy generation. In this context, the electricity network must rely on the upper power grid to provide a large amount of electricity to meet the large load demand, resulting in the lowest self-sustained rate (38.07%) under S1. S2 is designed to ensure that the power load in an HTES is satisfied as much as possible through sustainable energy generation. Consequently, a larger installed capacity of sustainable energy power plants is required under S2 to reduce the amount of power supplied from the upper power grid, thus ensuring that S2 maintains the highest self-sustained rate (55.72%). However, a large installed capacity makes the sustainable energy generation not fully consumed during certain periods. Consequently, the energy utilization rate under S2 (94.62%) is lower than that under S1 (99.68%). Moreover, a high energy utilization rate (99.32%) with a certain degree of self-sustained rate (45.26%) is ensured under S3. As discussed above, as there is a clear difference between planning schemes oriented toward different objectives, the planning schemes should be selected to meet local needs.

TABLE III
INSTALLED CAPACITY OF WIND AND PV POWER PLANTS
CONSTRUCTED IN EACH RASTER UNDER S1-S3

Raster	S1		S2		S3	
	S_i^w (kW)	S_i^{pv} (kW)	S_i^w (kW)	S_i^{pv} (kW)	S_i^w (kW)	S_i^{pv} (kW)
1	2000	0	2150	0	1850	0
2	0	0	0	0	0	0
3	0	0	0	0	0	0
4	2050	0	2100	0	1900	0
5	0	0	0	0	0	0
6	0	0	0	0	0	0
7	0	0	0	0	0	0
8	0	0	0	0	0	0
9	0	0	0	0	0	0
10	0	0	0	0	0	0
11	0	0	0	1200	0	0
12	0	0	0	1100	2150	0
13	1450	0	50	1750	0	1100
14	0	0	0	0	0	0
15	0	0	0	0	0	0
16	0	0	0	0	0	0
17	0	0	0	0	0	0
18	0	0	3600	3700	0	0
19	850	0	0	1100	350	4800
20	1550	0	0	1750	0	2500
21	0	0	0	0	0	0
22	0	0	0	0	0	0
23	0	0	0	0	0	0
24	0	0	0	0	0	0
25	0	0	0	0	0	0

TABLE IV
VALUES OF MULTIPLE OBJECTIVES UNDER S0-S3

Scheme	Total cost (\$)	Operation cost (\$)	Investment cost (\$)	Self-sustained rate (%)	Energy utilization rate (%)
S0	4.56×10^6	4.56×10^6	0	0	0
S1	4.05×10^6	2.80×10^6	1.25×10^6	38.07	99.68
S2	4.42×10^6	2.38×10^6	2.04×10^6	55.72	94.62
S3	4.10×10^6	2.48×10^6	1.62×10^6	45.26	99.32

In addition, Fig. 6 illustrates the siting schemes of the wind and PV power plants. According to the distribution of natural resources presented in Fig. 1, wind energy resources are more abundant in the northwestern and central parts of

the studied region, whereas solar energy resources are more abundant in the west-central part of the studied region. However, Fig. 6 shows that not all sustainable energy power plants are constructed in the most resource-rich locations. This is because the load distribution is different from that of sustainable energy resources. The demand in the east-central and northwestern parts of the highway is higher, as shown in

Fig. 3. Therefore, the sustainable energy power plants are mainly constructed in the northwestern, central, and eastern parts of the studied region to meet the demands of distributed loads. The above results illustrate that the siting schemes of sustainable energy power plants can effectively balance the differences between the distributions of sources and loads.

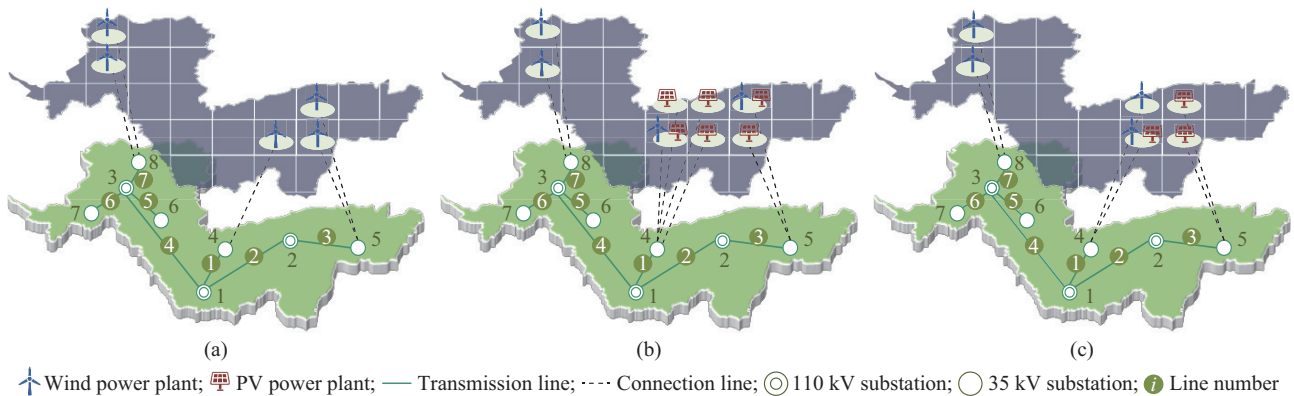


Fig. 6. Siting schemes for wind and PV power plants. (a) S1. (b) S2. (c) S3.

D. Analysis of Operation of Electricity-highway Network

The power balance of the entire HTES is presented in Supplementary Material A Fig. SA6. The sustainable energy generation is the main source of electricity supply, whereas the electricity from upper power grid is used as a supple-

ment. Energy storage also plays a role in power regulation by enhancing power consumption and compensating for power shortages. Tables V and VI show the self-sustained rate and energy utilization rate, respectively, which vary significantly on different typical days.

TABLE V
SELF-SUSTAINED RATE ON DIFFERENT TYPICAL DAYS

Scheme	Self-sustained rate (%)							
	Working day				Holiday			
	Spring	Summer	Autumn	Winter	Spring	Summer	Autumn	Winter
S1	48.57	13.56	29.85	71.71	41.26	11.80	27.05	60.81
S2	66.16	39.58	48.85	80.10	59.56	34.00	44.77	72.73
S3	56.14	31.37	38.61	68.34	47.19	27.08	35.70	57.62

TABLE VI
ENERGY UTILIZATION RATE ON DIFFERENT TYPICAL DAYS

Scheme	Energy utilization rate (%)							
	Working day				Holiday			
	Spring	Summer	Autumn	Winter	Spring	Summer	Autumn	Winter
S1	100.00	100	100.00	97.40	100.00	100	100	100.00
S2	85.73	100	96.82	86.47	94.28	100	100	93.68
S3	96.87	100	100.00	97.66	100.00	100	100	100.00

The specific differences are analyzed as follows.

1) The self-sustained rate on working days is slightly higher than that on holidays. As larger load demands on holidays put pressure on the electricity supply from sustainable energy power plants, the upper power grid provides more power to mitigate this pressure, leading to a lower self-sustained rate on holidays. According to Supplementary Material A Fig. SA5, the seasonal fluctuation in wind power is more significant than that in PV power. Overall, the generation capa-

bility of sustainable energy in summer and autumn is lower than that in spring and winter in the studied area, resulting in lower self-sustained rates in summer and autumn.

2) In terms of the energy utilization rate, a larger power demand on holidays promotes the consumption of more electricity from sustainable energy generation. Consequently, the energy utilization rate on holidays is higher than that on working days. In addition, the electricity from sustainable energy generation is higher in spring and winter, as shown in

Supplementary Material A Fig. SA5. However, higher electricity generation also indicates that electricity is more difficult to consume. Therefore, the energy utilization rates in spring and winter are lower than those in summer and autumn.

In addition, the curves shown in Supplementary Material A Fig. SA7 illustrate that the power flow of lines in electricity network exhibits an overall tendency to flow from nodes with small serial numbers to those with large serial numbers. This situation occurs primarily on lines 1 and 7. This is because sustainable energy power plants connected to nodes 4 and 8 can transmit excess power to other nodes via lines 1 and 7, respectively. Furthermore, to increase the self-sustained rate of HTES, the load power at each node should be met as much as possible by sustainable energy power plants connected to the electricity network. Therefore, the transmission power of lines 1 and 7 under S2 shows negative values at more moments than that under S1. Finally, the voltage fluctuation of each node under S2 is shown in Supplementary Material A Fig. SA8, indicating that the operation scheme corresponding to this planning scheme can effectively control the voltage fluctuation within a secure margin of $\pm 5\%$ of the rated voltage.

VI. CONCLUSION

This study develops a transformative multi-objective robust planning model tailored for the deployment of sustainable energy power plants along highways, with a particular focus on addressing intricate spatial-temporal variations in energy demands and resource availability. By employing advanced source-load-network cooperative operation models, we quantitatively characterize the energy distribution, facilitating precise decisions regarding the siting and sizing of wind and PV power plants. The contributions are threefold.

1) Quantitative analysis: the proposed planning model allows us to precisely map and utilize spatial-temporal distribution characteristics of source, which are particularly effective along the Xixiang Highway, where we observe significant variations in sustainable energy.

2) Efficiency in energy management: the adoption of source-load-network cooperative operation models facilitates the placement optimization of sustainable energy power plants, significantly promoting energy consumption and enhancing the efficiency of energy use near high-demand areas.

3) Adaptive multi-objective optimization: the developed multi-objective-oriented evaluation framework dynamically balances economic, environmental, and energy utilization metrics, showing variability in planning outcomes that respond flexibly to different weighting allocations.

Looking ahead, this study paves the way for further innovations.

1) Broadening energy sources: future studies will explore the integration of additional renewable sources, such as geothermal energy, tidal energy, and hydrogen, to enhance the sustainability of HTES.

2) Enhanced resilience models: incorporating the influence of multiple types of emergencies and extreme weather on electricity and highway networks will refine energy manage-

ment strategies, dynamically optimize distribution and consumption, and enhance HTES resilience.

In conclusion, this study not only fills vital gaps in the existing literature on HTES planning, but also sets forth a scalable structure for future sustainable developments in highway energy management. The comprehensive analysis and demonstrated practical viability underscore the transformative potential of the proposed planning model, providing a foundational blueprint for next-generation energy solutions in transportation infrastructure.

REFERENCES

- [1] International Energy Agency. (2017, Jul.). Global EV outlook 2017. [Online]. Available: <https://www.iea.org/reports/global-ev-outlook-2017>
- [2] Central People's Government of the People's Republic of China. (2021, Sept.). Comments on the complete, accurate and comprehensive implementation of the new development concept to well achieve carbon peak performance and carbon neutrality. [Online]. Available: https://www.gov.cn/gongbao/content/2021/content_5649728.htm
- [3] Central People's Government of the People's Republic of China. (2021, Feb.). Planning outline of national comprehensive and stereoscopic transportation network. [Online]. Available: https://www.gov.cn/zhengce/2021-02/24/content_5588654.htm
- [4] L. Jia, J. Ma, P. Cheng *et al.*, "A perspective on solar energy-powered road and rail transportation in China," *CSEE Journal of Power and Energy Systems*, vol. 6, no. 4, pp. 760-771, Dec. 2020.
- [5] M. S. Mahmud, M. W. Rahman, M. H. Lipu *et al.*, "Solar highway in Bangladesh using bifacial PV," in *Proceedings of 2018 IEEE International Conference on System, Computation, Automation and Networking*, Pondicherry, India, Jul. 2018, pp. 1-7.
- [6] S. Kim, Y. Lee, and H. Moon, "Siting criteria and feasibility analysis for PV power generation projects using road facilities," *Renewable and Sustainable Energy Reviews*, vol. 81, no. 2, pp. 3061-3069, Jan. 2018.
- [7] Popular Mechanics. (2017, Dec.). China is building a solar power highway. [Online]. Available: <https://www.popularmechanics.com/technology/infrastructure/a14479240/china-is-building-a-solar-powerhighway>
- [8] M. Xia, Y. Xian, and Q. Chen, "Collaborative planning for hybrid refueling stations with PV power in highway networks," *IEEE Transactions on Industry Applications*, vol. 60, no. 1, pp. 1219-1228, Jan.-Feb. 2024.
- [9] G. Yu, X. Zhang, H. Wang *et al.*, "Low carbon planning of PV-charging stations for self-sustained highway transportation energy system considering the retirement of gas stations," *IEEE Transactions on Industry Applications*, vol. 60, no. 1, pp. 1208-1218, Jan.-Feb. 2024.
- [10] R. Xie, W. Wei, M. E. Khodayar *et al.*, "Planning fully renewable powered charging stations on highways: a data-driven robust optimization approach," *IEEE Transactions on Transportation Electrification*, vol. 4, no. 3, pp. 817-830, Sept. 2018.
- [11] Y. Zhu, S. Li, and J. Tan, "Site selection and capacity determination of highway charging stations with photovoltaic energy storage," in *Proceedings of 2023 2nd Asia Power and Electrical Technology Conference*, Shanghai, China, Dec. 2023, pp. 846-850.
- [12] P. Zheng, Z. Fang, H. Li *et al.*, "Multi-objective optimization of hybrid energy management system for expressway chargers," *Journal of Energy Storage*, vol. 54, p. 105233, Oct. 2022.
- [13] M. Niu, H. Wang, J. Li *et al.*, "Coordinated energy dispatch of highway microgrids with mobile storage system based on DMPC optimization," *Electric Power Systems Research*, vol. 217, p. 109119, Apr. 2023.
- [14] D. Wang, H. Xu, L. Dai *et al.*, "Enhancing the utilization of renewable generation on the highway with mobile energy storage vehicles and electric vehicles," *Electric Power Systems Research*, vol. 231, p. 110311, Jun. 2024.
- [15] B. Li, H. Sun, J. Lou *et al.*, "An integration scheme for highway rest area integrating the distributed photovoltaic generation and energy storage," *IEEE Transactions on Industry Applications*, vol. 60, no. 1, pp. 1083-1092, Jan.-Feb. 2024.
- [16] R. Shi, K. Tang, and K. Y. Lee, "Optimal configuration of self-consistent microgrid system with hydrogen energy storage for highway service area," *IFAC-PapersOnLine*, vol. 56, no. 2, pp. 7960-7965, Jul. 2023.

- [17] L. Qi, P. Zheng, X. Wu *et al.*, "A hybrid wind-photovoltaic power generation system based on the foldable umbrella mechanism for applications on highways," *Solar Energy*, vol. 208, pp. 368-378, Sept. 2020.
- [18] M. Shi and Y. Huang, "Dynamic planning and energy management strategy of integrated charging and hydrogen refueling at highway energy supply stations considering on-site green hydrogen production," *International Journal of Hydrogen Energy*, vol. 48, no. 77, pp. 29835-29851, Sept. 2023.
- [19] R. Tang, N. Zhang, Z. Ma *et al.*, "Techno-economic evaluation of developing a zero-carbon highway service area energy system," *Energy Sources, Part A: Recovery, Utilization, and Environmental Effects*, vol. 46, no. 1, pp. 5552-5568, Apr. 2024.
- [20] C. Wang, C. Liu, J. Chen *et al.*, "Cooperative planning of renewable energy generation and multi-timescale flexible resources in active distribution networks," *Applied Energy*, vol. 356, p. 122429, Feb. 2024.
- [21] V. B. Pamshetti, S. Singh, A. K. Thakur *et al.*, "Cooperative operational planning model for distributed energy resources with soft open point in active distribution network," *IEEE Transactions on Industry Applications*, vol. 59, no. 2, pp. 2140-2151, Mar. 2023.
- [22] A. Avar and E. Ghanbari, "Optimal integration and planning of PV and wind renewable energy sources into distribution networks using the hybrid model of analytical techniques and metaheuristic algorithms: a deep learning-based approach," *Computers and Electrical Engineering*, vol. 117, p. 109280, Jul. 2024.
- [23] Y. Yang, J. Qiu, and C. Zhang, "Distribution network planning towards a low-carbon transition: a spatial-temporal carbon response method," *IEEE Transactions on Sustainable Energy*, vol. 15, no. 1, pp. 429-442, Jan. 2024.
- [24] Department of transportation of Sichuan province. (2024, Jul.). The two pilot projects carried out by Xixiang were selected as the first batch of special pilot projects for the construction of a green and low-carbon transport powerhouse by the Transport Ministry. [Online]. Available: <https://jtt.sc.gov.cn/jtt/c101587/2024/7/25/a3d8d82befa341d9b9f260f7e4d4e79d.shtml>
- [25] State-owned Assets Supervision and Administration Commission of Sichuan Province. (2024, Apr.). Transportation and energy integration increases motivation to the green and low-carbon construction of Xixiang highway. [Online]. Available: <https://gzw.sc.gov.cn/scsgzw/CU23020302/2024/4/17/ece777600ec746f8a967d2ac87338103.shtml>
- [26] B. Bacha, H. Ghodbane, H. Dahmani *et al.*, "Optimal sizing of a hybrid microgrid system using solar, wind, diesel, and battery energy storage to alleviate energy poverty in a rural area of Biskra, Algeria," *Journal of Energy Storage*, vol. 84, p. 110651, Apr. 2024.
- [27] T. Liu, J. Li, Z. Yang *et al.*, "Evaluation of the short- and long-duration energy storage requirements in solar-wind hybrid systems," *Energy Conversion and Management*, vol. 314, p. 118635, Aug. 2024.
- [28] H. Zhang, K. Liao, J. Yang *et al.*, "Frequency-constrained expansion planning for wind and photovoltaic power in wind-photovoltaic-hydrothermal multi-power system," *Applied Energy*, vol. 356, p. 122401, Feb. 2024.
- [29] Y. Song, M. Xia, L. Yang *et al.*, "Multi-granularity source-load-storage cooperative dispatch based on combined robust optimization and stochastic optimization for a highway service area micro-energy grid," *Renewable Energy*, vol. 205, pp. 747-762, Mar. 2023.
- [30] H. Zhu and H. Liu, "Fast local voltage control under limited reactive power: optimality and stability analysis," *IEEE Transactions on Power Systems*, vol. 31, no. 5, pp. 3794-3803, Sept. 2016.
- [31] B. Zeng and L. Zhao, "Solving two-stage robust optimization problems using a column-and-constraint generation method," *Operations Research Letters*, vol. 41, no. 5, pp. 457-461, Sept. 2013.
- [32] L. Song and G. Sheng, "A nonsmooth Levenberg-Marquardt method based on KKT conditions for real-time pricing in smart grid," *International Journal of Electrical Power & Energy Systems*, vol. 162, p. 110235, Nov. 2024.
- [33] A. Abdi, F. R. Astarai, and N. Rajabi, "GIS-AHP-GAMS based analysis of wind and solar energy integration for addressing energy shortage in industries: a case study," *Renewable Energy*, vol. 225, p. 120295, May 2024.
- [34] NASA. (2025, Apr.). Modern-era retrospective analysis for research and applications, Version 2. [Online]. Available: <https://gmao.gsfc.nasa.gov/gmao-products/merra-2/>

Gen Zhao received the B.S. degree in electrical engineering and automation from Sichuan University of Science & Engineering, Zigong, China, in 2011, and the M.S. degree in electrical engineering from Sichuan University, Chengdu, China, in 2017. He is currently working toward the Ph.D. degree in electrical engineering of Southwest Jiaotong University, Chengdu, China. His research interest includes integration of transportation and energy.

Huaiyuan Zhang received the B.S. degree in electrical engineering and automation from Southwest Jiaotong University, Chengdu, China, in 2021, where he is currently working toward the Ph.D. degree in electrical engineering. His research interests include integration of transportation and energy, and optimal planning and scheduling of sustainable energy system.

Jianhua Wang received the B.S. degree in electrical engineering and automation from Henan Polytechnic University, Jiaozuo, China, in 2022. He is currently working toward the Ph.D. degree in electrical engineering of Southwest Jiaotong University, Chengdu, China. His research interest includes integration of transportation and energy.

Zhengyou He received the B.S. and M.S. degrees in computational mechanics from Chongqing University, Chongqing, China, in 1992 and 1995, respectively, and the Ph.D. degree in electrical engineering from the School of Electrical Engineering, Southwest Jiaotong University, Chengdu, China, in 2001. He is currently a Professor with the School of Electrical Engineering, Southwest Jiaotong University. His research interests include integration of transportation and energy, fault diagnosis and reliability analysis for power systems, and high-speed railway traction power supply system.